ADVANCED FUNCTIONAL MATERIALS
www.afm-journal.de

Giant Magnetoresistance in a Molecular Thin Film as an Intrinsic Property

Luca Pilia, Michele Serri, Michio M. Matsushita, Kunio Awaga, Sandrine Heutz,* and Neil Robertson**

The magnetic, thin-film structural, conductivity, and magnetoresistance properties of [Ni(quinoline-8-thiolate)$_2$] ([Ni(qt)$_2$]) are studied. The conducting and magnetoresistance properties are studied in single crystals and in evaporated thin films through deposition on an interdigitated electrode array. Non-linear conductivity interpreted through a space-charge limited conduction mechanism with charges injected from the electrodes is observed. Under applied magnetic field, the material displays giant negative magnetoresistance above 50% at 2 K in both single crystals and in evaporated thin films. The effect can still be observed at 200 K and is interpreted in terms of a double exchange mechanism with the shape of the curve determined by the magnetic anisotropy. The unique observation of giant magnetoresistance (GMR) as an intrinsic effect in an evaporated thin film of paramagnetic molecules opens up new possibilities in organic spintronics.

1. Introduction

Since the discovery of giant magnetoresistance (GMR) in metallic multilayers in the 1980s, paving the way for modern magnetic data reading[1] and hybrid logic-storage devices,[2] the ability to manipulate and detect information using the electronic spin has attracted increasing interest in electronic materials.[3–7] Spintronics, and related phenomena combining charge transport with magnetic properties, can now be found in inorganic, organic and single-molecule materials and devices showing phenomena including magnetoresistance,[8] switching,[9] memory effects[10] and aimed towards quantum information processing.[11] Alongside these developments, electronic materials comprising organic or molecular building blocks has exploded into an enormous academic and industrial field including light-emitting devices, photovoltaics, and transistors.[12] The combination of spintronics with organic materials therefore presents a key emerging challenge. The approach of using non-magnetic organic spacers between ferromagnets in a spin-valve structure[8,13,14] is a promising approach but presents challenging interface (or so-called "spinterface") engineering.[15–17] Also, magnetoresistance (MR) has been observed in organic diode structures with non-magnetic electrodes but these still require detailed interpretation.[18]

An attractive alternative involves use of paramagnetic molecular materials to achieve GMR as this represents a property that is intrinsic to the material itself rather than dependent on the interface, and is well understood through a double-exchange mechanism.[19] In related fields, multifunctional molecular materials incorporating paramagnetic molecules[20] have led to a rich series of phenomena, including room-temperature magnetic bistability[21], non-linear conductivity,[22] field-induced superconductivity,[23,24] conducting ferromagnets[25] and radical-based conductors.[26,27] Regarding GMR in paramagnetic molecular materials however, prior work has been limited to only two families; [TPP][Fe(phthalocyanine)L$_2$]$_2$ (L = CN, Cl, Br) and related crystalline salts;[28–30] and nitronyl nitroxide-tetrathiafulvalene molecules,[19,31–33] all studied in the form of brittle single-crystals. The development of molecular materials in practical devices however, requires solution- or vapor-processed polycrystalline or amorphous thin films.[34] In this context, we report our observation of GMR in vapor-processed films of paramagnetic [Ni(qt)$_2$] (**Figure 1**), which opens up new directions in the design of molecular spintronic materials and their application as thin films in devices.

2. Results and Discussion

[Ni(qt)$_2$] forms chains where molecules are linked through intermolecular S–Ni bonds, with two inequivalent chains oriented along the a-axis (Figure 1). Within this structure, Ni(II)

Dr. L. Pilia, Dr. N. Robertson
EaStCHEM School of Chemistry
University of Edinburgh King's Buildings
West Mains Road, Edinburgh, EH9 3JJ, UK
E-mail: neil.robertson@ed.ac.uk
M. Serri, Dr. S. Heutz
Department of Materials and
London Centre for Nanotechnology
Imperial College London
Exhibition Road, London, SW7 2AZ, UK
E-mail: s.heutz@imperial.ac.uk
Prof. M. M. Matsushita, Prof. K. Awaga
Department of Chemistry
Graduate School of Science
and Research Center of Materials Science
Nagoya University
Chikusa-ku, Nagoya, 464–8602, Japan
E-mail: mmmatsushita@nagoya-u.jp

DOI: 10.1002/adfm.201303218

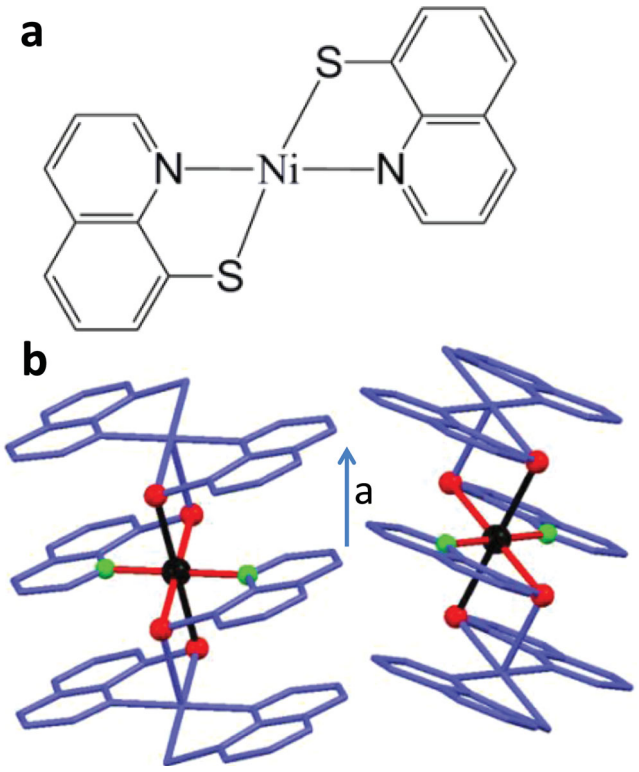

Figure 1. a) molecular structure of $[Ni(qt)_2]$. b) chains along the *a*-axis formed through axial Ni(II)...S interactions. The coordination sphere of selected Ni atoms is highlighted (Ni black, S red, and N green). The chelate coordination is shown with red bonds and the longer axial interactions with black bonds.

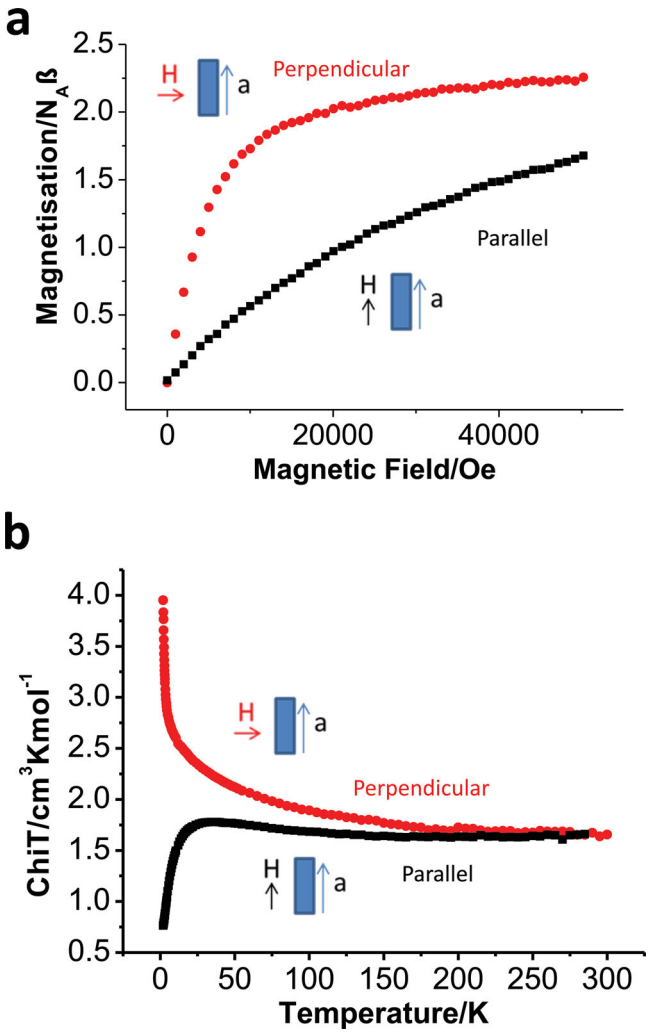

Figure 2. Comparison between magnetization measurements on crystals aligned perpendicular (red circles) and parallel (black squares) to the applied magnetic field. a) Magnetization as a function of field at 2 K. b) χT product against temperature at field of 1000 Oe.

is in a distorted octahedral environment, where the sulfur and nitrogen atoms of the ligands adopt a *trans* geometry within the equatorial plane. Previous studies have highlighted a weak ferromagnetic interaction and the lack of magnetic saturation at fields up to 70 kOe, attributed to single-ion anisotropy or a spin canted structure.[35,36] These magnetic properties, in addition to a strong electron-donating character of $[Ni(qt)_2]$ in charge transfer salts,[36] are promising ingredients for MR behavior and prompted our further study.

2.1. Structural and Magnetic Properties

Firstly, to gain deeper insight into the magnetic anisotropy, we compare crystals aligned perpendicular and parallel to the applied magnetic field. The crystals have a needle-like shape, with the a-axis, and therefore the chains, aligned along the long direction (referred to hereafter as the parallel orientation). The χT products for the parallel and perpendicular orientations diverge below 200 K (**Figure 2**) indicating significant anisotropy, with preferential orientation of the magnetic moments in the perpendicular direction. The g-factor derived from the high-temperature χT value is 2.53. This is larger than 2.26 reported in the literature,[36] but the discrepancy can be attributed to the ≈ 10% error in determining the mass of the small single crystal. In keeping with the susceptibility data, the magnetization (Figure 2 and Supporting Information, Figure S1) for parallel crystals increases incrementally with the field, while the perpendicular orientation shows a rapid rise at low temperature although it does not reach saturation at 50 kOe. This again indicates easier magnetization along the perpendicular direction. The a.c. magnetic susceptibility showed no significant out-of-phase signal down to 2 K, indicating no evidence of spin-glass or single-chain-magnet behavior, consistent with lack of long range order down to 2 K.[37]

As discussed above, a key requirement for the implementation of organic-based technology is the ability to process the materials as thin films. We were able to evaporate the material for the first time using organic molecular beam deposition on a range of substrates including, for example, kapton, silicon, and glass. The films display facetted particles with sizes above 100 nm that homogeneously cover the substrate (**Figure 3**) and show a distinctive diffraction pattern (**Figure 4**) on all substrates (Figure S3, Supporting Information). By randomizing

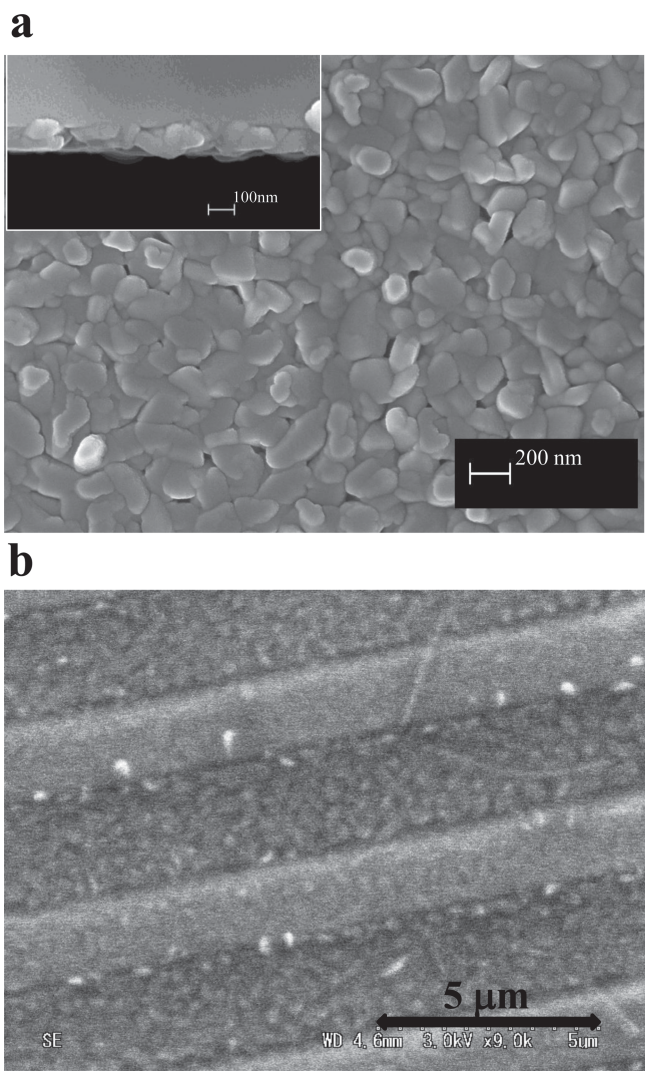

Figure 3. a) SEM image of a 75 nm thick film on Si (inset: cross-section). b) SEM image of the interdigitated Pt-electrode array with deposited $[Ni(qt)_2]$.

the orientation of the particles of a 400 nm thick film, we identified a range of peaks, with the main reflections occurring at 9.8°, 11.6°, and 22.8°, indicating strong preferential orientation within the film on the substrate. The peak positions differ from those of the bulk material[35] indicating a different phase, however conversion of the film to the bulk structure upon annealing (Figures S4,S5, Supporting Information) was observed.

The magnetic characterization of a 75 nm film on kapton, reveals an S = 1 system (Figure S2, Supporting Information) which, alongside the ready interconversion through annealing, strongly suggests a similar chain structure to the bulk phase that probably differs only in the chain orientations. At 25 K, the magnetic data are accurately modelled using the Brillouin function, however at lower temperatures the magnetization is significantly reduced compared to the isotropic spin model (Figure S2, Supporting Information), and lower than either parallel or perpendicular magnetization of the crystals. In addition, the curve at 2 K shows a rise at low field that is more rapid

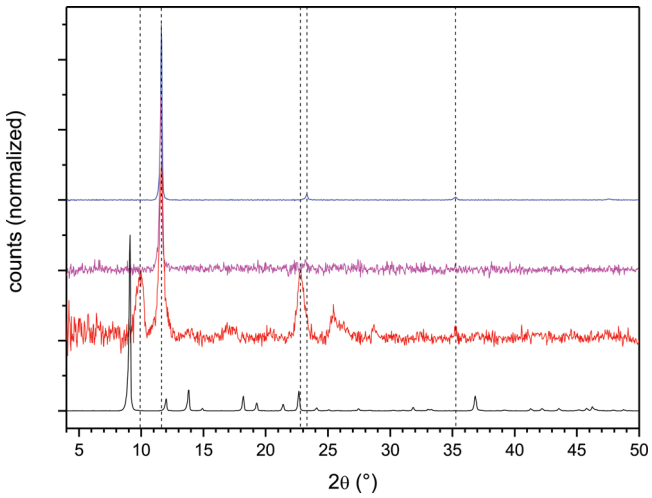

Figure 4. Comparison of out of plane XRD measurements of [Ni(qt)2]: powder before evaporation (black), powder scratched from a 400 nm film (red), thin film (75 nm) on glass (magenta), 400 nm film on glass (blue). The pristine powder XRD pattern corresponds with that calculated from the single crystal X-ray data.[35]

than the Brillouin function suggesting the presence of weak ferromagnetism. These factors point to strong anisotropy of the Ni(II) centres that differs in magnitude from that of the powder data.

2.2. Conductivity and Magnetoresistance

Conductivity of the thin film and of $[Ni(qt)_2]$ single-crystals parallel and perpendicularly-aligned to the current direction were studied on an interdigitated electrode substrate (**Figure 5** and Supporting Information, Figures S6,S7). All film and crystal samples showed current versus voltage (*I*–*V*) characteristics with strong non-linear behavior (Figure 5). The currents are

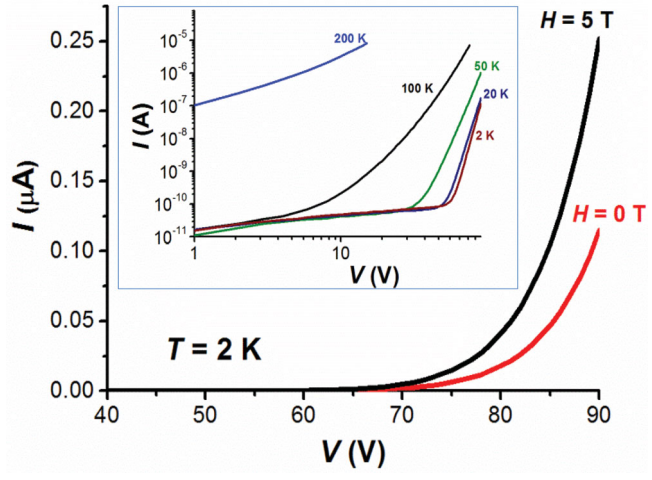

Figure 5. Magnetic field dependence of *I*–*V* at 2 K for crystals aligned parallel to the magnetic field; the inset shows the non-linear *I*–*V* behavior for the same device.

very low with low bias voltage, however above a threshold value (≈60 V at 2 K) increase exponentially. Similar results were obtained by Komatsu et al.[19] in the case of a tetrathiafulvalene-nitronyl nitroxide radical, and the non-linear behavior explained as a result of a space-charge-limited conduction (SCLC) mechanism[38,39] with carriers injected from the electrodes. For $[Ni(qt)_2]$, the strong electron-donor property[36] suggests that the injected carriers are holes. Above the threshold voltage, the *I–V* behavior can be modelled by an exponential law ($I \propto V^{m+1}$) (Figure 5), with *m* ranging from 1 to 14 at 200 and 2 K respectively, confirming that the current is dominated by a trapped-charge-limited conduction (TCLC) regime within the SCLC mechanism. In these conditions, the current is due to the bulk properties of the compound rather than the contact effects.

The MR effect was measured on the same devices by varying the magnetic field between –5 and 5 T and applying a constant bias voltage, chosen in each case to give a conveniently measureable current within the non-linear region. To avoid the appearance of the Lorentz force the experiment was set up with the magnetic field parallel to the current direction. **Figure 6** shows the magnetic field dependence of resistance of the $[Ni(qt)_2]$ complex in the oriented crystalline phases and the thin film phase reported as a percentage $(R–R_{0T})/R_{0T}$, where *R* and R_{0T} are the resistance with and without applied magnetic field, respectively. It is apparent that $[Ni(qt)_2]$ shows giant negative magnetoresistance in both phases and in both crystal orientations. At 2 K the resistance decreases more than 60% for the crystals and 50% for the thin film, and the effect is still important (10%) at 50 K. Moreover, it is still possible to observe the MR effect up to 200 K, although it has decreased below 1% (Figure S8, Supporting Information) suggesting that the degree of exchange interaction between the spin of the conduction electrons and those localized at the metal ions is around 200 K. Alternatively, the temperature of the MR may be limited by the magnetization since the MR is proportional to the square of the magnetization for the double exchange mechanism (vide infra).[31]

2.3. Calculations and Discussion

Calculations at the unrestricted B3LYP/6–31G(d) level of theory were performed on an 8-mer of the chain, with the length chosen to approximate the spin correlation length at low temperature.[35] These show a fully occupied HOMO possessing predominantly ligand character (Figure S9, Supporting Information) with SOMO orbitals from the unpaired spins at lower energy, consistent with observations in nitronyl nitroxide-tetrathiafulvalene molecules.[19] As would be expected, the spin density is predominantly located around the Ni(II) centre (Figure S10, Supporting Information). At high applied electric field, hole doping of the HOMO band occurs, giving rise to a system involving hole transport via the HOMO orbitals based on the quinoxaline ligands, occuring in the presence of the unpaired SOMO spins centred on the Ni(II) centres.

A double exchange mechanism can be used to explain the observed MR as follows. An applied magnetic field will align the localized SOMO spins (Figure 6d) which will couple with the HOMO electrons on the same small-molecule unit. This gives alignment of the spins of the HOMO electrons between neighbouring molecular units, leading to hole hopping with reduced scattering since favorable spin alignment is maintained upon hole transfer. The strong coupling between the HOMO and SOMO spins, due to co-location on a small molecular unit, is consistent with the MR effect persisting to high temperatures.

For the double-exchange mechanism, the MR should scale with the square of the magnetization.[31] A comparison was made of MR with magnetization-squared, both plotted against field for the single-crystal data at 2 K, the conditions under which the curves showed the most distinct shape (Figure S11, Supporting Information). For both parallel and perpendicular crystal orientations, a clear correlation was shown between the MR and magnetization-squared, providing strong evidence for the double-exchange mechanism. The crystals show ferromagnetic interactions, however any extended spin correlation does not persist above a few K and MR persists well above 100 K, hence the

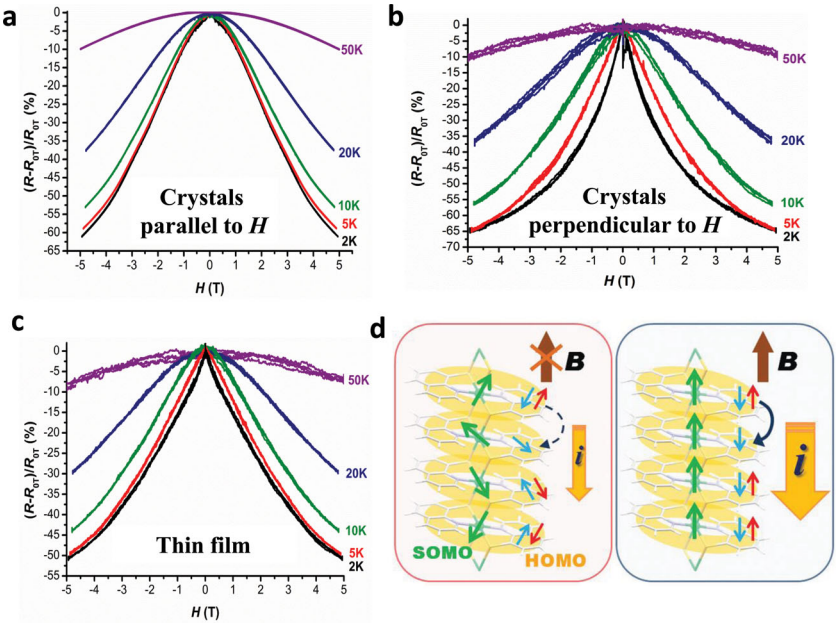

Figure 6. Magnetic field dependence of the magnetoresistance of $[Ni(qt)_2]$ at various temperatures on a) crystals parallel to *H* and aligned perpendicularly to interdigitated Pt electrodes with 2 µm gap; bias voltage 60 V; b) crystals perpendicular to *H*; bias voltage 85 V; c) on thin film deposited onto an identical interdigitated device; bias voltage 75V. d) Schematic of the double-exchange mechanism for the GMR. Green arrows show localized unpaired spins of the S = 1 centre, red arrows show the α-HOMO electrons and blue arrows show the β-HOMO electrons. The location of the arrows is not representative of the spin density. Calculations indicate the α-electron of the HOMO to be significantly higher in energy than the β-electron hence we show the α-electron to be removed when the hole forms.

ferromagnetic exchange is unlikely to be a prerequisite for the MR effect, although it may have an impact on the magnitude and anisotropy of the MR at low temperature (Figure S11, Supporting Information).

We note that for the thin-film MR curve, the shape more closely resembles the perpendicular crystal orientation, probably related to the preferred orientation shown within the thin films (Figure S3, Supporting Information). Also noteworthy, is that the MR shown in the film phase is of comparable magnitude to that of the single crystals, despite the presence of grain boundaries in the film. Although the anisotropy of the magnetization is important in determining the shape of the MR curve, it is apparent that both crystal orientations can display MR to a broadly comparable extent. In fact, the lack of strong dependence on crystal orientation, and the small effect of grain boundaries, are key aspects in MR of the thin-film, which is composed of crystallites where the orientation is likely to be random within the substrate plane (and therefore the current direction), despite the out-of-plane texture.

3. Conclusion

In conclusion, we have observed for the first time giant negative magnetoresistance in a vapor-deposited molecular thin film. The GMR property is intrinsic to the material and not dependent on interface engineering and in this regard falls into the family of small-paramagnetic-molecule GMR materials previously observed using either nitronyl-nitroxide-tetrathiafullerenes or Fe-phthalocyanines. Notably however, [Ni(qt)2] is only the second example in the field where no doping and hence no counterion was required, and thus since the material is not a salt, vapor deposition into a thin film was able to be achieved. This ability to deposit [Ni(qt)2] as a thin-film demonstrates for the first time that the GMR effect can be observed as an intrinsic property in the type of evaporated polycrystalline film widely applied in the field of organic electronics. The opportunity to build on this finding and develop new materials with related properties opens a new chapter in the joint development of the spintronics and the organic electronics fields towards practical devices.

4. Experimental Section

Materials Synthesis and Film Growth: All chemicals were purchased from Sigma Aldrich and used without further purification. [Ni(qt)$_2$] was prepared as previously reported [35]. Anal. calcd for $C_{18}H_{12}N_2NiS_2$: C 57.02, H 3.19, N 7.39; found: C 56.90, H 3.08, N 7.28. Deposition of [Ni(qt)$_2$] thin films for XRD and magnetic characterization was carried out using a SPECTROS OMBD system by Kurt J. Lesker at a growth rate of 0.2 Å s^{-1}, at a pressure of 5×10^{-5} Pa (base pressure 10^{-7} mbar). Devices and films used for the annealing study were prepared via physical vapor deposition (PVD) with sources held in a temperature range between 461 °C and 488 °C at a pressure of 6.8×10^{-4} Pa. This resulted in a growth rate of 0.1–0.2 Å s^{-1} which was monitored using a quartz crystalmicrobalance (QCM). The materials to be sublimed were heated inside an inert crucible by applying a current. Films of 100 nm thickness were produced according to the QCM. The actual film thickness was measured using a profilometer and using the optical absorption of the dissolved film calibrated using solutions of known concentration.

Characterization: Thin film XRD was carried out on a Rigaku ultraX-18HB at room temperature. Data were collected from 2θ angle of 5–50° at a rate of 3° per minute. Images of the crystal structures were produced using Mercury 2.3.[40] Magnetic susceptibility measurements were performed using a Quantum Design MPMS-XL SQUID magnetometer with MPMS MultiVu Application software to process the data. The temperature dependence of transport properties including magnetoresistance were carried out by utilizing the cryostat of the SQUID magnetometer equipped with a handmade transport probe. Keithley 2487 picoammeter was used for both voltage application and current detection. The measurements were carried out in the dark and under vacuum using a Keithley 2636A sourcemeter equipped with Labtracer 2.0 software. All the conductivity and magnetoresistance measurements were performed on platinum interdigitated electrodes as source and drain, deposited onto a quartz surface with a width of 2 μm and a gap of 2 μm. For the experiments with the crystalline phase the devices were prepared mounting crystals of 1–2 mm length and several μm of width, onto Pt electrodes. Imaging of thin films was carried out using a Hitachi S-4300 Scanning Electron Microscope.

Computational: Calculations were performed with Gaussian 09 Rev. C01, using the unrestricted B3LYP functional and 6–31G(d) basis set with spin multiplicity of the octomer set for 17 to model the ferromagnetic segment and using the crystal structure geometry [35] without further optimization. Mercury and Winmostar V3.8 (TENCUBE Institute, Ltd) were used for preparing the molecular coordination and Gaussian input file. MolStudio R4.0 Rev 2.0 program (NEC Corporation) was used for generating MOs and Spin Density images.

Supporting Information

Supporting Information is available from the Wiley Online Library or from the author.

Acknowledgements

L.P. thanks the EU Marie Curie programme for funding. The authors thank the EPSRC Global project EP/K004468; the EPSRC project EP/G049726; the Japanese Science and Technology agency; the Leverhulme Trust and the JSPS Core-to-Core programme for supporting the UK-Japan collaboration. M.S. and S.H. thank EPSRC for the grant EP/H002022/1.

Received: September 17, 2013
Revised: November 4, 2013
Published online: December 16, 2013

[1] M. N. Baibich, J. M. Broto, A. Fert, F. Nguyen Van Dau, F. Petroff, P. Eitenne, G. Creuzet, A. Friederich, J. Chazelas, *Phys. Rev. Lett.* **1988**, *61*, 2472.
[2] D. D. Awschalom, M. E. Flatté, *Nat. Phys.* **2007**, *3*, 153.
[3] S. Sanvito, *Chem. Soc. Rev.* **2011**, *40*, 3336.
[4] T. D. Nguyen, E. Ehrenfreund, Z. V. Vardeny, *Science* **2012**, *337*, 204.
[5] S. D. Jiang, K. Goss, C. Cervetti, L. Bogani, *Sci. China* **2012**, *55*, 867.
[6] P. P. Freitas, F. A. Cardoso, V. C. Martins, S. A. M. Martins, J. Loureiro, J. Amaral, R. C. Chaves, S. Cardoso, L. P. Fonseca, A. M. Sebastião, M. Pannetier-Lecoeur, C. Fermon, *Lab Chip* **2012**, *12*, 546.
[7] G. Li, S. Sun, R. J. Wilson, R. L. White, N. Pourmand, S. X. Wang, *Sens. Actuators A: Phys.* **2006**, *126*, 98.
[8] Z. H. Xiong, D. Wu, Z. V. Vardeny, J. Shi, *Nature* **2004**, *427*, 821.
[9] A. Rotaru, I. A. Guralskiy, Gabor Molnar, L. Salmon, P. Dermont, A. Bousseksou, *Chem. Commun.* **2012**, *48*, 4163.

[10] J. Lee, E. Lee, S. Kim, G. Sook Bang, D. A. Shultz, R. D. Schmidt, M. D. E. Forbes, H. Lee, *Angew. Chem. Int. Ed.* **2011**, *50*, 4414.
[11] L. Bogani, W. Wernsdorfer, *Nat. Mater.* **2008**, *7*, 179.
[12] A. C. Arias, J. D. MacKenzie, I. McCulloch, J. Rivnay, A. Salleo, *Chem. Rev.* **2010**, *110*, 3.
[13] J.-W. Yoo, H. W. Jang, V. N. Prigodin, C. Kao, C. B. Eom, A. J. Epstein, *Phys. Rev. B* **2009**, *80*, 205207.
[14] J.-W. Yoo, C.-Y. Chen, H. W. Jang, C. W. Bark, V. N. Prigodin, C. B. Eom, A. J. Epstein, *Nat. Mater.* **2010**, *9*, 638.
[15] P. Ruden, *Nat. Mater.* **2001**, *10*, 8.
[16] D. Sun, L. Yin, C. Sun, H. Guo, Z. Gai, X.-G. Zhang, T. Z. Ward, Z. Cheng, J. Shen, *Phys. Rev. Lett.* **2010**, *104*, 236602.
[17] L. Schulz, L. Nuccio, M. Willis, P. Desai, P. Shakya, T. Kreouzis, V. K. Malik, C. Bernhard, F. L. Pratt, N. A. Morley, A. Suter, G. J. Nieuwenhuys, T. Prokscha, E. Morenzoni, W. P. Gillin, A. J. Drew, *Nat. Mater.* **2011**, *10*, 39.
[18] T. L. Francis, Ö. Mermer, G. Veeraraghavan, M. Wohlgenannt, *New J. Phys.* **2004**, *6*, 185.
[19] H. Komatsu, M. M. Matsushita, S. Yamamura, Y. Sugawara, K. Suzuki, T. Sugawara, *J. Am. Chem. Soc.* **2010**, *132*, 4528.
[20] I. Ratera, J. Veciana, *Chem. Soc. Rev.* **2012**, *41*, 303.
[21] W. Fujita, K. Awaga, *Science* **1999**, *286*, 261.
[22] K. Okamota, T. Tanaka, W. Fujita, K. Awaga, T. Inabe, *Phys. Rev. B.* **2007**, *76*, 075328.
[23] S. Uji, H. Shinagawa, T. Terashima, T. Yakabe, Y. Terai, M. Tokumoto, A. Kobayashi, H. Tanaka, H. Kobayashi, *Nature* **2001**, *410*, 908.
[24] H. Fujiwara, H. Kobayashi, E. Fujiwara, A. Kobayashi, *J. Am. Chem. Soc.* **2002**, *124*, 6816.
[25] E. Coronado, J. R. Galan-Mascaros, C. J. Gomez-Garcia, V. Laukhin, *Nature* **2000**, *408*, 447.
[26] A. Sarkar, M. E. Itkis, F. S. Tham, R. C. Haddon, *Chem. Eur. J.* **2011**, *17*, 11576.
[27] S. M. Winter, A. R. Balo, R. J. Roberts, K. Lekin, A. Assoud, P. A. Dube, R. T. Oakley, *Chem. Commun.* **2013**, *49*, 1603.
[28] N. Hanasaki, M. Matsuda, H. Tajima, E. Ohmichi, T. Osada, T. Naito, T. Inabe, *J. Phys. Soc. Jpn.* **2006**, *75*, 033703.
[29] D. Ethelbhert, C. Yu, M. Matsuda, H. Tajima, T. Naito, T. Inabe, *Dalton Trans* **2011**, *40*, 2283.
[30] D. Ethelbhert, C. Yu, M. Matsuda, H. Tajima, A. Kikuchi, T. Taketsugu, N. Hanasaki, T. Naito, T. Inabe, *J. Mater. Chem.* **2009**, *19*, 718.
[31] M. M. Matsushita, H. Kawakami, T. Sugawara, M. Ogata, *Phys. Rev. B* **2008**, *77*, 195208.
[32] M. M. Matsushita, H. Kawakami, Y. Kawada, T. Sugawara, *Chem. Lett.* **2007**, *36*, 110.
[33] T. Sugawara, H. Komatsu, K. Suzuki, *Chem. Soc. Rev.* **2011**, *40*, 3105.
[34] N. Crivillers, M. Mas-Torrent, C. Rovira, J. Veciana, *J. Mater. Chem.* **2012**, *22*, 138833.
[35] T. Miyake, T. Ishida, D. Hashizume, F. Iwasaki, T. Nogami, *Chem. Lett.* **2000**, 952.
[36] T. Miyake, T. Ishida, D. Hashizume, F. Iwasaki, T. Nogami, *Polyhedron* **2001**, *20*, 1551.
[37] F-P. Huang, J.-L. Tian, D.-D. Li, G.-J. Chen, W. Gu, S.-P. Yan, X. Liu, D.-Z. Liao, P. Cheng, *Inorg. Chem.* **2010**, *49*, 2525.
[38] K. C. Kao, W. Hwang, *Electrical Transport in Solids*, Pergamon Press, Oxford **1981**.
[39] P. E. Burrows, Z. Shen, V. Bulovic, D. M. McCarty, S. R. Forrest, J. A. Cronin, M. E. Thompson, *J. Appl. Phys.* **1996**, *79*, 7991.
[40] C. F. Macrae, I. J. Bruno, J. A. Chisholm, P. R. Edgington, P. McCabe, E. Pidcock, L. Rodriguez-Monge, R. Taylor, J. van de Streek, P. A. Wood, *J. Appl. Cryst.* **2008**, *41*, 466.